Chaos Induced by Magnetic Field in Asymmetric Double Barrier Resonant Tunneling Structures

F. Claro
Facultad de Fisica, Pontificia Universidad Católica de Chile
Vicuna Mackenna 4860, Casilla 306, Santiago 22, Chile

P. Orellana*
Centro Brasileiro de Pesquisas Físicas,
Rua Dr. Xavier Sigaud 150, Urca 2290-180 Rio de Janeiro-RJ, Brazil

and

E. Anda
Instituto de Física, Universidad Federal Fluminense,
Av. Gal. Milton Tavares s/n, Gragoata, 2421-340 Niteroi, RJ, Brazil

Received July 21, 1995

We show that a transition to chaos is expected in an asymmetric double barrier structure with a magnetic field parallel to the current. The transition occurs via successive bifurcations as the magnetic field is increased. The origin of this chaotic behavior is the electron-electron interaction in the space between the barriers near resonance.

Since the first observation of resonant tunneling through semiconductor based double barrier structures by Chang, Esaki and Tsu, these devices have been found to exhibit a variety of interesting physical properties[1]. Besides a peak due to simple resonant transmission, structures arising from phonon[2] and plasmon -assisted[3] resonant tunneling, as well as from Landau level matching[4,5], has been observed. Moreover, an intrinsic dynamical bistability and hysteresis in the negative differential resistance region has been reported[4,6,7]. These latter effects arise from the Coulomb repulsion experienced by incoming electrons from the charge buildup in the space between the barriers[6]. Numerical simulations show the system to oscillate as states of unstable electron charge buildup and ejection are reached[8]. In this work we include a magnetic field parallel to the current and explore the unstable region as the field is increased. We show that, while the phenomenon of hysteresis persists, the system bifurcates into bistability, and is capable of further bifurcations leading to true chaos.

We consider the transport properties of a double barrier heterostructure in the presence of a longitudinal magnetic field. A tight-binding model is used for the electron Hamiltonian. The response of the system is studied introducing a fully selfconsistent scheme to treat the electron-electron interaction in the steady state when the bias is applied. Inclusion of a longitudinal magnetic field B (in the growth direction, henceforth called the z direction) is simple if a parabolic energy dispersion parallel to the interfaces is assumed. The field quantizes the motion of the electrons in the xy plane, giving rise to Landau levels with energies $\epsilon_n = (n + 1/2)\hbar\omega_c$, where $n = 0, 1, 2, ...$ is the Landau

*Actual address: Universidad de Santiago de Chile, Departamento de Física, Casilla 307, Santiago, Chile.

index and $\omega_c = eB/m^*c$ is the cyclotron frequency. Assuming that the longitudinal degree of freedom is decoupled from the transverse motion the hamiltonian takes the form,

$$H = \sum_{in\sigma}(\epsilon_i + \epsilon_n)c^{\dagger n}_{i\sigma}c^n_{i\sigma} + t\sum_{<ij>n\sigma} c^{\dagger n}_{i\sigma}c^n_{j\sigma} + \sum_{ijkln\sigma\sigma'} U^{ij}_{kl}c^{\dagger n}_{i\sigma}c^n_{j\sigma'}c^{\dagger n}_{k\sigma}c^n_{l\sigma'} \ , \quad (1)$$

where the operator $c^\dagger_i$ creates an electron at site i in a Landau level n, t is the hopping matrix element between nearest neighbors $< ij >$, ϵ_i the band contour and external bias, and U^{ij}_{kl} the electron-electron coupling matrix. For simplicity we have restricted the Coulomb interaction to the intrasite contribution and we ignored the spin degree of freedom. A Zeeman splitting of the Landau levels can easily be included in our model, yet we shall ignore them here. As in the Hubbard model we have assumed the Coulomb repulsion of the electrons to be represented by its dominant term, the intra-atomic interaction. Although there is no essential difficulty in incorporating the inter-atomic contributions, the numerical calculation is more involved, without introducing qualitative differences in the physical description of the system.[9]

The eigenstates may be expanded in an orthonormal basis of states localized at site i corresponding to Landau level n of the noninteracting single electron system $|i, n >$,

$$|\psi^\alpha >= \sum_l a^{n\alpha}_i |i, n > \quad (2)$$

Here

$$a^{n\alpha}_i =< i, n|\psi^\alpha >=< 0|c^n_i|\psi^\alpha > \quad (3)$$

with $|0 >$ representing the vacuum. Applying the Hamiltonian (1) on the wave function (2) the eigenvalues equation results to be

$$\epsilon_\alpha a^{n\alpha}_i = (\epsilon_i + \epsilon_n + U\sum_{n\beta}|a^{n\beta}_i|^2)a^{n\alpha}_i = t(a^{n\alpha}_{i-1} + a^{n\alpha}_{i+1} - 2a^{n\alpha}_i) \quad (4)$$

where the sum over β covers all occupied electron states of the system. We have used a mean field approximation (Hartree) to treat the electron-electron interaction, the energy ϵ_α is measured from the bottom of the band. This is a nonlinear difference equation for the coefficients $a^{n\alpha}_i$, its nonlinear character arising from the thirth term in the right hand side.

Equation (4) has the usual form for a tight binding band, except for the presence of external fields and the nonlinear interaction in the diagonal term. In order to study its solutions we assume a plane wave incident from the left, which is partly reflected and partly transmitted by the device. The waveform at the far right is a single plane wave and the iteration of Eq. (4) may thus be conveniently done from right to left. For a given transmitted amplitude the associated reflected and incident amplitudes may be determined by matching the iterated function to the proper plane waves at the far left. We assume the sample has a total of N sites.

Because of the presence of the nonlinear term in Eq. (4) it is convenient to define a second time-like iteration in the following way. Initially Eq. (4) is solved ignoring the nonlinear term and for energies up to the Fermi energy. The coefficients thus obtained correspond to a solution for non interacting electrons. They are used to construct the nonlinear term for the next solution (second time-iterate) of Eq. (4). The procedure is continued, always using for the nonlinear term solutions of the previous time-iteration. This procedure defines the spatio-pseudo-temporal map,

$$\epsilon_\alpha a^{n\alpha}_{i,\tau+1} = (\epsilon_i + \epsilon_n + U\sum_{n\beta}|a^{n\beta}_i|^2)a^{n\alpha}_{i,\tau+1} = t(a^{n\alpha}_{i-1,\tau+1} + a^{n\alpha}_{i+1,\tau+1} - 2a^{n\alpha}_{i,\tau+1}) \ , \quad (5)$$

that is linear in space (i) and nonlinear in time (τ). Maps nonlinear in space and time have been studied in other contexts. In particular, the coupled map model for open flow has been found to exhibit spatial chaos with temporal periodicity[10]. As we shall see, in our case chaos develops in the time iterates, only. Note however that the time variable here is fictitious since Eq. (4) describes the stationary solutions and we are not solving the time dependent problem explicitely. In

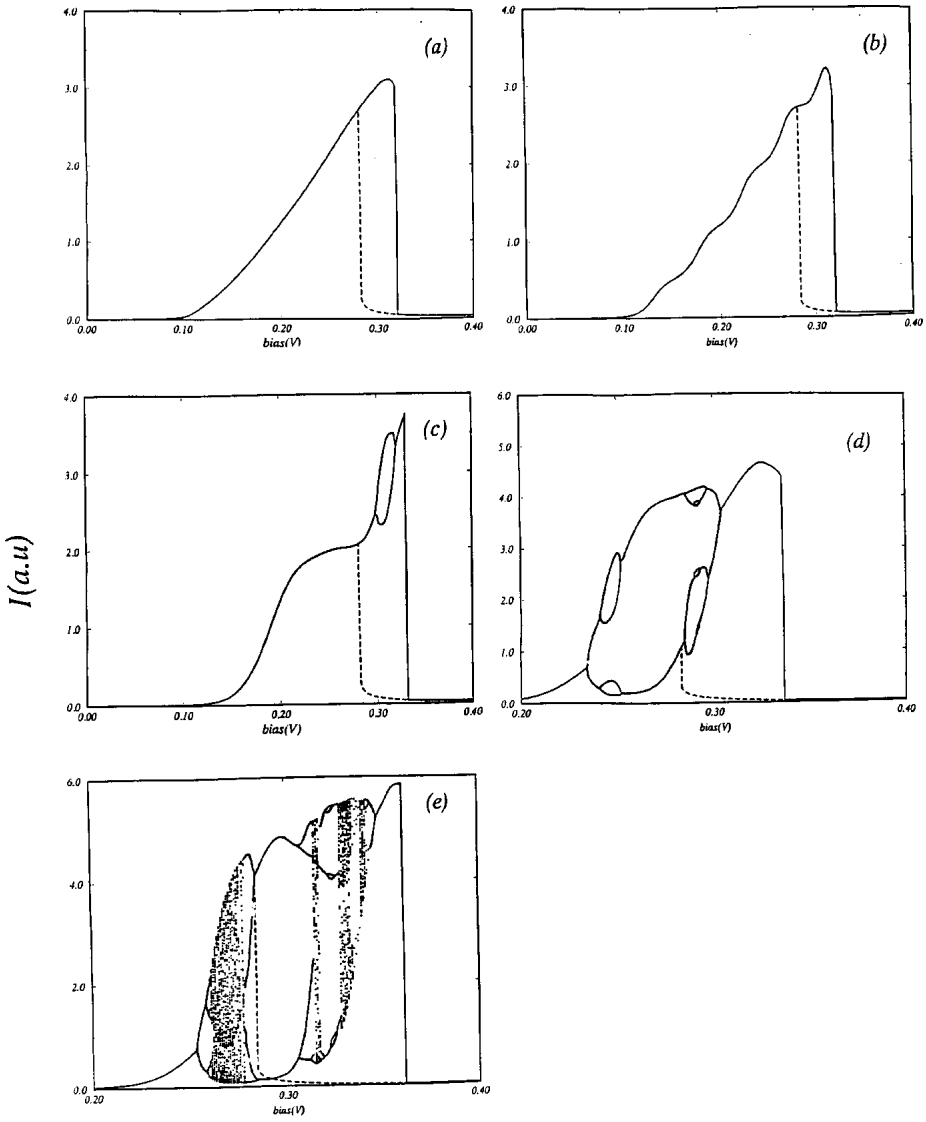

Figure 1. Current-voltage characteristics for a) B = 0T, b) B = 2T, c) B = 6T, d) B = 13T and e) B = 17T. Dashed lines are for decreasing bias. Sample parameters for this and following figures are described in the text.

fact our procedure is what is usually referred to as a self-consistent loop. From the coefficients obtained solving Eq. (4) we compute the current using the expression[11]

$$J = \frac{e}{\hbar(\pi l_m)^2} \sum_n \int_0^{k_{nf}} k_z' |T|^2 dk_z \ , \qquad (6)$$

where $l_m = (\hbar c/eB)^{1/2}$ is the magnetic length, $|T| = |a_N|$ the transmission coefficient of the normalized eigenstate at energy ϵ, ϵ_f the Fermi energy, $k_z(k_z')$ is de magnitude of the electron wave vector in the emitter (collector), $k_{nf} = \sqrt{2m^*/\hbar^2(\epsilon_f - \epsilon_n)}$ and the sum is over magnetic energies $\epsilon_n \leq \epsilon_f$.

For definiteness we apply our model in what follows to an asymmetric GaAs/AlGaAs double barrier structure, with emitter and collector barrier thicknesses of 1.12nm (2 sites) and 3.36nm, (6 sites) respectively, and a well thickness of 11.2nm (20 sites). For this geometry the first resonance at zero bias occurs at 30 meV. The conduction band offset is set at 300 meV. The buffer layers are uniformly doped up to 3nm from either barrier, and so as to give a neutralizing free carrier concentration of $2 \times 10^{17}\text{cm}^{-3}$ at the contacts. In equilibrium and at B = 0T, the Fermi level lies 19.2meV above the asymptotic conduction band edge, so the zero bias resonance lies above the Fermi sea. The external potential is taken to drop linearly between the left edge of the first barrier and 112 sites down to the right. The parameter values in Eq. (4) are set at t = 2.16eV and U =

10meV, appropriate for GaAs[12]. The sample has N = 400 points and the normalization of the wave functions is chosen so that charge from the electrons filling up to the Fermi energy exactly cancels the positive charge at the contacts. In our procedure the map is linear in space, so that normalization involves simple multiplication of all coefficients at a given energy by a constant. Since the electron density has rather long range oscillations we made sure the sample was long enough to make finite size effects small. We solved Eq. (4) using the procedure described above, for an energy mesh appropriate to compute the integral in Eq. (7). Good convergence was found for a mesh of 100 points.

Fig. 1 shows the current-voltage (I-V) characteristics for several values of the magnetic field. At zero field hysteresis is obtained as the voltage is increased (Fig. 1(a), solid line), and later decreased (dashed line). In either case the time iteration was found to converge to a stable fixed point. The width W of the hysteresis loop is enhanced by our choice of an asymmetric structure, with a collector barrier that is wider than the emitter barrier, as expected[13,14]. Calling $r = w_L/w_R$ the ratio between our left and right barriers we increased w_R keeping all other parameters fixed and found W to rise smoothly from zero at $r = 0.9$, and saturate to W = 0.077V at $r = 0.55$.

When the magnetic field is turned on, oscillations in the I-V curve appear as the bias is increased, as seen previously in other samples both in experimental[5] as well as theoretical[15] work. They are illustrated in Fig 1(b) for B = 2T. These oscillations may be associated with Landau levels in the 2D space between the barriers entering the Fermi sea and opening new channels for conduction. A completely novel feature starts to develop at B = 4.8T, however, where two period-two fixed-points are encountered in the time iteration at certain voltages. This bubble-like feature is illustrated in Fig. 1(c) for B = 6T. Note that these new solutions are not reached as the voltage is decreased (dashed line). This suggests that the bistable regime and the hysteresis effect correspond to two different attractors of the nonlinear map. At 6T there are two Landau levels occupied so a single shoulder appears in this figure. As the magnetic field is raised still further the area of the bistable bubble decreases and finally disappears. A new bubble sets in however at B = 6.5T and 0.18V. At larger fields it undergoes further bifurcations, as seen for B = 13T in Fig. 1(d), and finally full chaos appears as shown for B = 17T in Fig. 1(e).

A better display of the transition to chaos is obtained in an I-B diagram, as shown in Fig. 2(a) for a fixed bias of 0.27V. At low magnetic field the current oscillates with the field, a feature that has been observed experimentally and arises from the oscillations in the Fermi energy[4]. A thin bifurcation loop appears at 5T, corresponding to the loop seen in Fig. 1(c), which has moved to lower bias with increasing B. At higher fields the current undergoes a bifurcation cascade leading to a chaotic region, which eventually unfolds back to solutions of finite periodicity. The last 500 points of a 1000 iteration run are shown. The Lyapunov exponents associated with this figure are shown in Fig. 2(b). They were obtained using the method of Wolf et al [16].

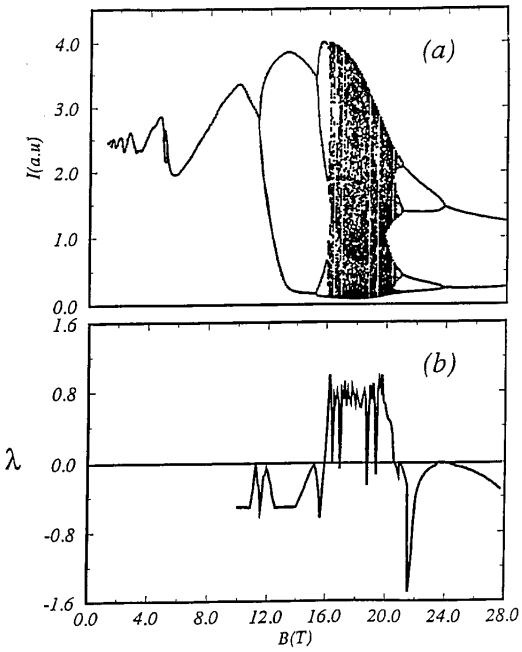

Figure 2. I-B diagram (a) and Lyapunov exponent (b) for a fixed bias of 0.27V.

Fig. 3 shows the dimensionless charge density $S = \sum_\beta |a_i^\beta|^2$ across the sample in the chaotic region for 0.27V and 17T. Included in the figure are time iterations form $\tau = 200$ to $\tau = 400$. Note that only points to the left of the barriers are significantly affected by the chaotic behavior of the system. The solution with little charge between the barriers, shown in more detail in the inset of the figure, was obtained decreasing the voltage from above, and gives the hysteresis effect.

As noted above, it is not accessible when the voltage increases, suggesting that hysteresis and multi-stability or chaos are separate phenomena.[8]

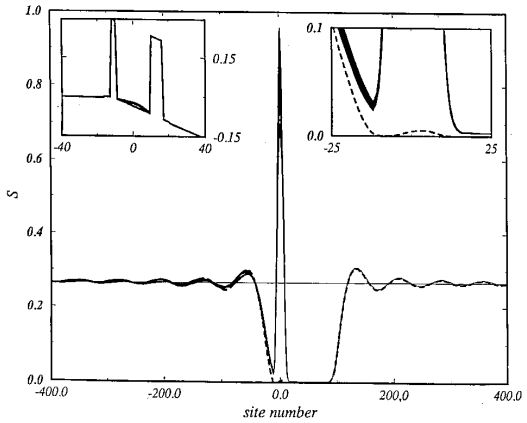

Figure 3. Dimensionless charge density S in the chaotic region for 0.27V and 17T. Right inset shows detail of the figure. Left inset shows the potential profile in eV.

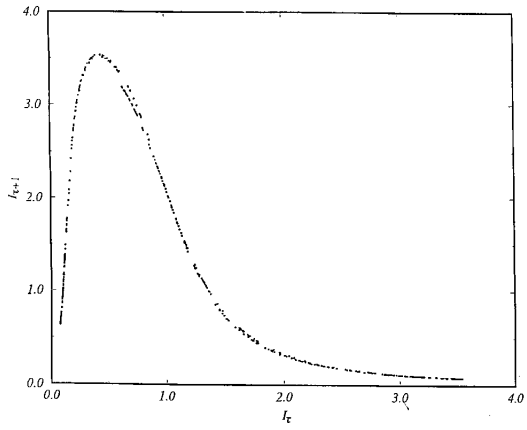

Figure 4. Iteration map for the current at 0.27V and 18T.

The current is a global property of the spatial map we are considering, in the sense that it is invariant in space and involves a convolution of solutions at all relevant energies. In our procedure for solving Eq. (4) it defines a sequence $I^{B,V} + \tau + 1 = f(I_\tau^{B,V})$ which sets up a two-parameter one-dimensional map in the problem. The shape of the map may be obtained from the time series in the chaotic region at fixed bias and magnetic field. An example is shown in Fig. 4, at 0.27V and 18T. A map with the same shape characterizing the Belousov- Zhabotinskii reaction has been shown to describe a strange attractor[17]. We note however that the shape is not universal in all chaotic regions of parameter space.

Fig. 5 is a phase diagram in the two parameter space V-B showing the various structures we have described. The thick lines delimit the region of hysteresis. In the dotted regions bifurcations of various orders appear, while the brick design marks regions where chaos is present. The horizontal dashed line at 0.27V guides the eye in identifying the structure exhibited in Fig. 2, while the vertical line at B = 17T may be used to follow the complex structure found in Fig. 1(e). It is clear from the figure that there are wide regions of experimentally accesible values of the bias and magnetic field where chaos is present, which opens the interesting possibility of an experimental study of the transition to chaos in a mesoscopic device.

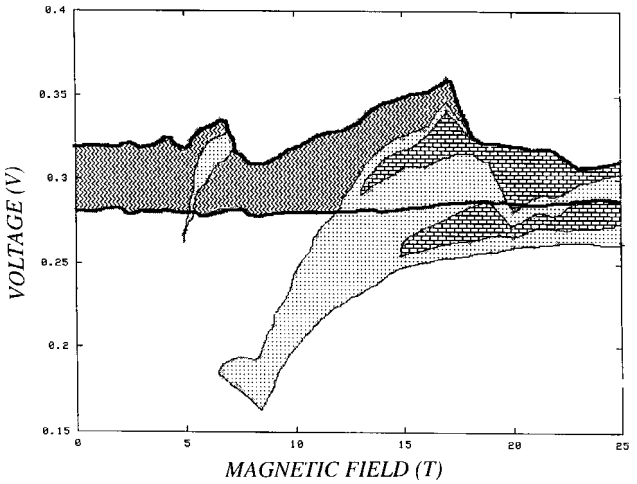

Figure 5. Phase diagram in parameter space. The thick lines delimit the region of hysteresis. Dotted areas are where one or more bifurcations are present while the brick design marks chaotic regions. The vertical (horizontal) dashed line corresponds to Fig. (1e) (Fig. (2a)).

In summary, we have shown that an asymmetric double barrier near resonance is capable of undergoing a transition to chaos through the route of bifurcations. We characterize the associated nonlinear map by the current, and use as control parameters the bias and the magnetic field, all easily measurable quantities. It is hoped that this work will motivate an experimental search of the predicted transition.

Acknowledgments

One of us (FC) would like to thank H. Cerdeira for an illuminating discussion. This work was supported in part by CNPq, CLAF, FINEP, and FONDECYT, grant 1930553,

References

1. L. L. Chang, L. Esaki and R. Tsu, Appl. Phys. Lett. **24,** 593 (1974).
2. V. J. Goldman, D. C. Tsui and J. E. Cunningham, Phys. Rev. **B36**, 7635 (1987).
3. C. Zhang, M. L. F. Lerch, A. D. Martin, P. E. Simmonds and L. Eaves, Phys. Rev. Lett. **72**, 3397 (1994).
4. A. Zaslavsky, V. J. Goldman, D. C. Tsui and J. E. Cunningham, Appl. Phys. Lett. **53**, 1408 (1988).
5. A. Zaslavsky, D. C. Tsui, M. Santos and M. Shayegan, Phys. Rev. **B40**, 9829 (1989).
6. V. J. Goldman, D. C. Tsui and J. E. Cunningham, Phys. Rev. Lett. **58**, 1256 (1987).
7. T. C. L. G. Sollner, Phys. Rev. Lett. **59**, 1622 (1987).
8. K. L. Jensen and F. A. Buot, Phys. Rev. Lett. **66**, 1078 (1991).
9. J. Hubbard, Proc. R. Soc. London, **A276**, 238 (1963).
10. F. H. Willeboordse and K. Kaneka, Phys. Rev. Lett. **73**, 533 (1994).
11. D. D. Coon and H. C. Liu, Appl. Phys. Lett. **47**, 172 (1985).
12. G. Bastard, in: *Wave Mechanics Applied to Semiconductor Heterostructures* (Les éditions de physique, 1988) p. 34.
13. C. R. H. White, M. S. Skolnick, L. Eaves and M. L. Leadbeater, Appl. Phys. Lett. **58**, 1164 (1991).
14. P. L. Pernas, F. Flores and E. V. Anda, Phys. Rev. **B47**, 4779 (1993).
15. W. Potz, Phys. Rev. **B41**, 12111 (1990).
16. A. Wolf, J. Swift, H. Swinney and J. Vastano, Physica **7D** 285 (1985).
17. J. C. Roux, R. H. Simoyi and H. L. Swinney, Physica **8D**, 257 (1983).
18. N. Kamata, K. Yamada, N. Miura and L. Eaves, Physica **B184**, 250 (1993)